Holocene water balance variations in Great Salt Lake, Utah: application of GDGT indices and the ACE salinity proxy

Rachel T. So[1*], Tim K. Lowenstein[2], Elliot Jagniecki[3], Jessica E. Tierney[4], Sarah J. Feakins[1]

[1]Department of Earth Sciences, University of Southern California, Los Angeles, CA 90089, USA.

[2] Department of Geological Sciences and Environmental Studies, State University of New York, Binghamton, NY 13902, USA.

[3]Utah Geological Survey, Salt Lake City, UT 84114, USA.

[4]Department of Geoscience, University of Arizona, Tucson, AZ 85721, USA.

*Corresponding author: Rachel T. So (rtso@usc.edu)

Key Points:

- Glycerol dialkyl glycerol tetraethers produced by bacteria and archaea can detect Holocene limnological changes at Great Salt Lake.
- Based on the Archaeol-Caldarchaeol Ecometric salinity index, Great Salt Lake has remained hypersaline from 7.2 ka to present.
- A 5.5 ka step shift in several proxies is likely correlated to a regional decrease in aridity during the mid-late Holocene transition.

Abstract

Great Salt Lake (UT) is a hypersaline terminal lake in the US Great Basin, and the remnant of the late glacial Lake Bonneville. Holocene hydroclimate variations cannot be interpreted from the shoreline record, but instead can be investigated by proxies archived in the sediments. GLAD1-GSL00-1B was cored in 2000 and recently dated by radiocarbon for the Holocene section with the top 11 m representing ~7 ka to present. Sediment samples every 30 cm (~220 years) were studied for the full suite of microbial membrane lipids, including those responsive to temperature and salinity. The ACE index detects the increase in lipids of halophilic archaea, relative to generalists, as salinity increases. We find Holocene ACE values ranged from 81-98, which suggests persistent hypersalinity with <50 g/L variability across 7.2 kyr. The temperature proxy, MBT_{5Me}, yields values similar to modern mean annual air temperature for months above freezing (MAF = 15.7°C) over the last 5.5 kyr. Several GDGT metrics show a step shift at 5.5 ka before which temperature estimates are unreliable due to the shift in lake ecology and likely shallow depth. The step change in lake conditions at 5.5 ka and additional variations within the late Holocene are compared to regional climate records. We find evidence for a dry mid-Holocene in GSL, corroborating other records.

Keywords: GDGT, ACE, Holocene, Great Salt Lake

Plain Language Summary

Great Salt Lake in Utah is the remnant of a much larger lake and is currently at a historically low level. We study a lake sediment core, collected in 2000 from the floor of Great Salt Lake, and recently dated. We take new samples from the core and measure them for molecules made by microbes, whether living in the lake or washed in from the surrounding soils. We reconstruct lake conditions during the last 7,000 years and assess whether lake level fluctuated during that time. Over the past 7,200 years, we find evidence that the lake was shallower from 7,200 to 5,500 years ago, but has been relatively stable until the modifications of the lake in the 20th Century and the current drying trend.

1. Introduction

Modern day Great Salt Lake (GSL) is a remnant of the Pleistocene freshwater paleolake, Lake Bonneville. Lake Bonneville began rising at ~30 cal ka BP, reaching its maximum size (~52,000 km^2) at ~18 cal ka BP and forming the Bonneville shoreline (Oviatt et al., 2021). Afterwards, continued downcutting at the outflow point eventually caused rapid overflow during the Bonneville flood, dropping lake levels by 100 m. This was followed by a regressive phase where evaporation caused the lake to reach modern GSL levels by ~13 cal ka BP. Except for a brief 15 m rise at 12 cal ka BP (locally known as the Gilbert Episode), GSL levels have probably remained steady at around 1,280 masl (m above sea level) during the Holocene (Oviatt et al., 2021).

Yet, there have been climate fluctuations within the Holocene. In the early Holocene (~11 to ~8 cal ka BP), parts of the southwestern US experienced a wet interval resulting in lake high stands at Tulare Lake (CA) (Blunt and Negrini, 2015) and Lake Elsinore (CA) (Kirby et al., 2007). Owens Lake (CA) is less consistent, with low lake levels reconstructed prior to 9 cal ka BP (Bacon et al., 2020; Benson et al., 2002). Further inland, Lehman Caves (NV) speleothem records indicate wet conditions during the early Holocene (Steponaitis et al., 2015), but records from Leviathan Cave (NV) (Lachniet et al., 2020) suggest a warm and arid early Holocene in the Bonneville Basin, with no detected human settlements (Goebel et al., 2021).

In the middle Holocene (~8 to ~4 cal ka BP) much of western interior North America experienced dry conditions. Lake low stands or desiccation occurred at Owens Lake (Bacon et al., 2020; Benson et al., 2002), Lake Tahoe (CA/NV) (Benson et al., 2002), Pyramid Lake (NV) (Benson et al., 2002), six Midwestern lakes west of the Great Lakes (Shuman et al., 2002), and in five small sub-alpine lakes (WY, CO) in the Rocky Mountains (Shuman and Serravezza, 2017). Arid conditions were also recorded at Lehman Caves (Steponaitis et al., 2015) and Leviathan Cave (Lachniet et al., 2020).

The late Holocene (~4 ka to present) was cooler and wetter than the middle Holocene, but with oscillations between droughts and pluvials. From ~4.5 to ~3 cal ka BP, high stands were recorded at Owens Lake (Bacon et al., 2020; Benson et al., 2002), Walker Lake (NV) (Benson et al., 1991), Pyramid Lake (NV) (Briggs et al., 2005), Winnemucca Lake (NV) (Briggs et al., 2005), Mono

Lake (CA) (Stine, 1990), Silver Lake (CA) (Enzel et al., 1989), and several small Rocky Mountains lakes (Shuman and Serravezza, 2017). There seems to be evidence of the Late Holocene Dry Period (2.8-1.85 cal ka BP) proposed by Mensing et al. (2013) with lake low stands at Mono Lake (Stine, 1990), Walker Lake (Adams, 2007; Benson et al., 1991), Zaca Lake (CA) (Kirby et al., 2014), and Bear Lake (UT/ID) (Moser and Kimball, 2009).

While the shift between the wet early Holocene and dry middle Holocene has been linked to the decrease in summer insolation (Bird and Kirby, 2006; Kirby et al., 2007; Lachniet et al., 2020) and the decline of the Laurentide Ice Sheet (LIS) (Shuman et al., 2002; Shuman et al., 2006; Steponaitis et al., 2015), there is additional variability besides the long term trend. However, understanding of Holocene variability is hampered by apparent spatial differences, varied responses between different proxies, and/or insufficient age control, leaving uncertainty in the comparisons between archives (Oviatt et al., 2015).

Continuous geochemical records from sediment cores have potential to reconstruct Holocene climate when shoreline records are lacking. In the hypersaline GSL, salinity is of primary interest for limnological reconstructions. Archaeol and caldarchaeol concentrations are used to calculate the Archaeol-Caldarchaeol Ecometric (ACE), originally developed to track the contrasting salinity of marine, hypersaline, estuarine, and freshwater environments (Turich and Freeman, 2011). Archaeol is a diphytanyl glycerol diether primarily produced by halophilic *Euryarchaeota* (Dawson et al., 2012; Macalady et al., 2004; Teixidor et al., 1993), and caldarchaeol is an isoprenoid glycerol dialkyl glycerol tetraether (isoGDGT) produced by *Crenarchaeota*, *Thaumarchaeota*, and some *Euryarchaeota* (Schouten et al., 2013). An increase in salinity leads to an increase in ACE values, reflecting the shift from a cosmopolitan archaeal community to a halophilic community. The ACE index has been tested in modern sediments in lakes of varying salinities (He et al., 2020; Wang et al., 2013) and used for past hydroclimate reconstructions at Lake Elsinore (CA) and Searles Lake (CA) (Feakins et al., 2019; Peaple et al., 2022). Other isoGDGT compounds can reveal aspects of paleolimnology and past archaeal productivity.

Branched GDGTs (brGDGTs), biomarkers produced by bacteria, have also been widely applied to lacustrine sediments including for temperature reconstructions (e.g. Martinez-Sosa et al., 2021). A recent calibration study on subalpine (>2,700 masl) Rocky Mountain lakes of varying depth found complications with the brGDGT temperature proxy related to lake depth and stratification (Stefanescu et al., 2021). They found shallow lakes (<7 m) were well mixed in summer whereas deeper lakes remained stratified with cold bottom waters. At-depth production of brGDGTs appeared to explain correlations with lake bottom water temperatures, fixing the temperature signals in deep lakes, whereas shallower lakes recorded local air temperatures (Stefanescu et al., 2021). In contrast, GSL is a lower elevation (1,280 masl), hypersaline lake with density controlled primarily by salinity rather than temperature. GSL has fluctuated between 7.6 m and 13.7 m deep over the historical record (1847-present) (Belovsky et al., 2011) and

lake levels may have been even lower during the more arid times of the Holocene. Therefore, lake level fluctuations may influence the brGDGT signal, although the limnological and ecological patterns are unlikely to match those of the high elevation freshwater lake calibration of Stefanescu et al. (2021). Beyond lake level fluctuations, other concerns are that the high salinity environment of GSL may create complications with application of the existing calibrations (Martinez-Sosa et al., 2021).

Here, we use biomarkers to study Holocene paleoenvironments at GSL, targeting iso- and brGDGTs. We test now widely used proxies on an extreme environment and track climate change and limnological conditions in GSL throughout the middle to late Holocene. In August 2022, GSL lake levels were at a surface elevation of 1,277 m, 3 m below the historic average of 1,280 m (Ramirez, 2022). Current trends of drought in the region and diversion of inflowing rivers for human consumption (Wurtsbaugh et al., 2017) are projected to lead to further declines in lake levels in the coming decades. The decreasing areal extent of GSL is leaving infrastructure at abandoned shorelines leading to reduced access for tourism and recreation. There are growing concerns over health effects associated with exposed lakebed dust (Null and Wurtsbaugh, 2020; Perry et al., 2019). In the lake, the increase in salinity will alter ecosystems, which currently provide habitats for migratory shore and water birds (Jewell, 2021; Sorensen et al., 2020). Changing salinities and lake access will also affect existing resource extraction, in particular the brine shrimp cyst and mineral extraction industries (Naftz, 2017; Wurtsbaugh et al., 2017). Here, we seek to reconstruct a 7 kyr hydroclimate history of GSL to better understand the natural range of variability within the Holocene climate state and provide a longer context for current drying trends.

1. Study location

Great Salt Lake (GSL) is a hypersaline terminal lake located in Utah in the eastern part of the United States' Great Basin (**Figure 1**). At the lake's historic mean elevation of 1,280 masl, the lake is more than 10 m deep across the central part of the basin and averages 5.5 m deep (Belovsky et al., 2011; Shope and Angeroth, 2015). In 2000, the Global Lakes Drilling (GLAD) initiative drilled four sites to a total of 120 m below lake floor reaching back to the boundary of oxygen isotope stages 6 and 7 (~175 ka) (Dinter et al., 2000). The original study reported density, magnetic susceptibility, minerology, inorganic carbon, and organic carbon from the recovered cores (Dinter et al., 2000). Recently the Holocene sedimentary section in the upper 11 m of GLAD1-GSL00-1B (41.094°N, 112.365°W, 8.4 m water depth) was dated using radiocarbon (Bowen et al., 2019). The Holocene sedimentary sequence is the target for the biomarker reconstructions here.

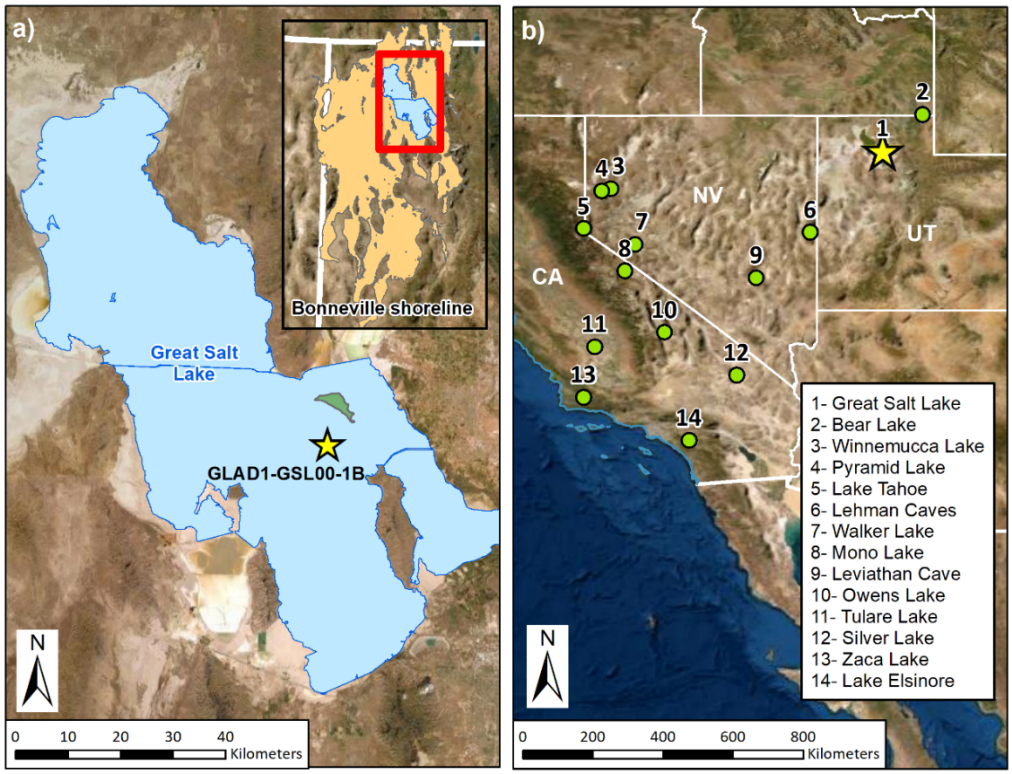

Figure 1. Maps showing a) the Great Salt Lake (GSL) core site of GLAD1-GSL00-1B and the Lake Bonneville shoreline (top right), and b) the locations of regional comparison records.

The lake water balance includes inflow from rivers (66%), precipitation (31%), and groundwater (3%) and leaves by evaporation from the closed basin (Jones et al., 2009). Instrumental records from 1966 to present indicate 7 m of fluctuation in lake levels (Rupke and McDonald, 2012; United States Geological Survey, 2022b) due to the changing water balance. During the high stand of the last glacial maximum/Heinrich Stadial 1 (HS1), GSL occupied a much greater areal extent, up to ~52,000 km^2, forming the freshwater Lake Bonneville (Baxter et al., 2005; Oviatt et al., 2021). The drier climate since then has led to the formation of the Bonneville Salt Flats (west of the present-day GSL) and a reduction of the lake size to <10% of its former extent.

Riverine inflow to the GSL primarily comes from the Bear (32.5 ± 34.4 m^3/s), Jordan (3.5 ± 1.2 m^3/s), and Weber Rivers (8.1 ± 15.9 m^3/s; all reported as 2000-2020 annual mean discharge). The Bear River records low discharge (2-5 m^3/s) in the dry summer months from July to September, with flow rising

consistently during the fall to a plateau of 20-50 m^3/s in January and February. Peak flows occur in March to April, reaching >50 m^3/s, and then drop back down to 2-5 m^3/s by June (United States Geological Survey, 2022a).

The modern GSL is separated into a northern and southern section by a railroad causeway built in 1959. As rivers exclusively flow into the South Arm of GSL, salinities there today are 120-180 g/L, whereas the North Arm has salinities of 290-340 g/L and a permanent halite bottom crust (data for 2010-2021, Jagniecki et al., 2021; Rupke and McDonald, 2012). Salinity is heterogeneous around the shallow lake margins with freshwater influence near river inflows and evaporative enrichment along other margins. At times, a halocline has been measured in depth profiles in the south arm, but at present the lake is not stratified (Rupke and McDonald, 2012). Since the North Arm resembles a restricted evaporation pond, South Am conditions are likely representative of the pre-causeway GSL (Belovsky et al., 2011).

1. **Age model**

Bowen et al. (2019) measured the radiocarbon of various materials (including brine shrimp cysts, algal mats, *n*-alkanes, carbonate, total organic carbon, and terrestrial macrofossils) from the GSL sediment core GLAD1-GSL00-1B and formulated a radiocarbon age model based upon the cysts only (n = 15 dates). While some components are older (carbonates) or younger (charcoal), we are interested in all the organics that formed in the lake waters as age control for the lake biomarker-based record. In addition to cysts, the short chain *n*-alkanes, algal mats, and total organic carbon (TOC) all appear to form in lake waters. Thus, these additional age constraints are used to inform a revised age model here (n = 27 dates, **Figure 2a**), which is modestly different from the prior age model (**Figure 2b**). The revised age model produces older ages (300 years) between 5.5 and 3 ka (**Figure 2c**).

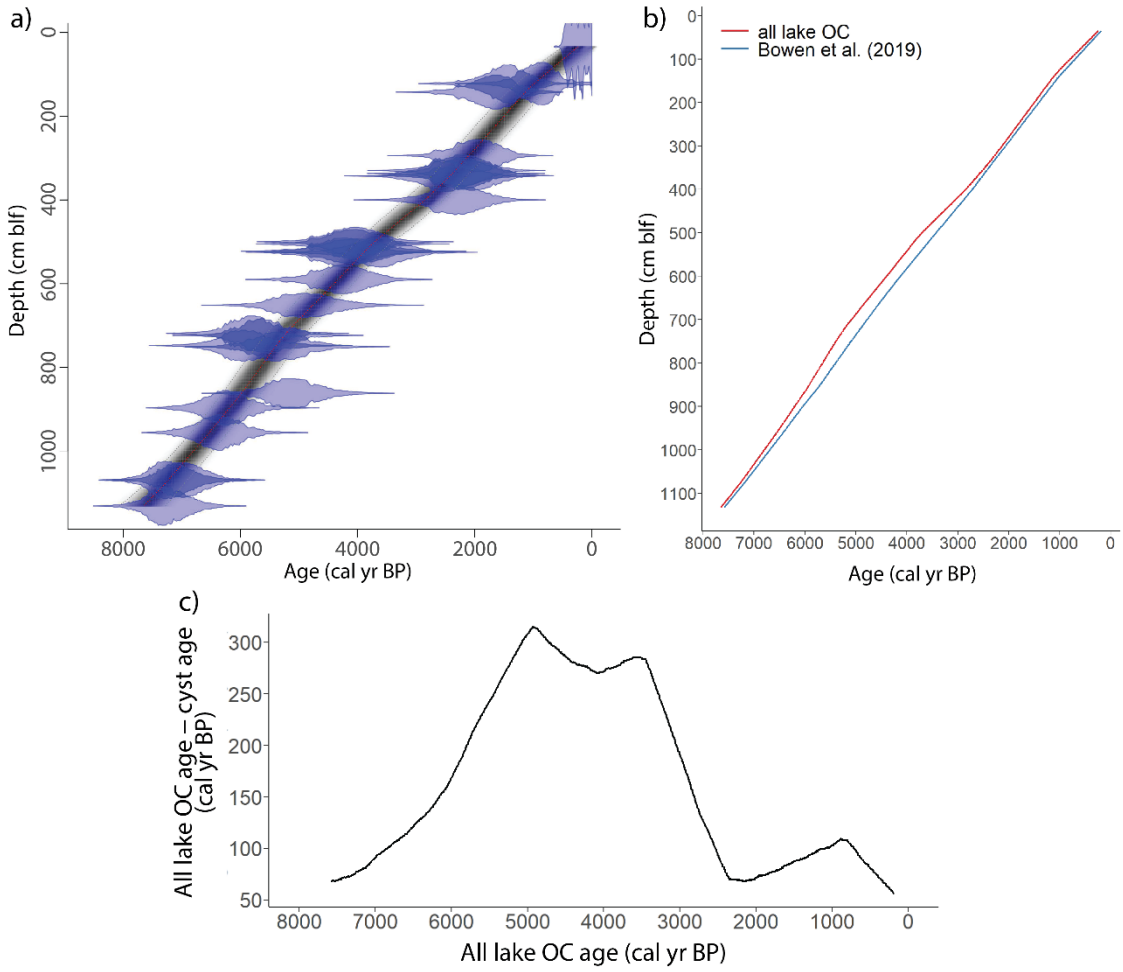

Figure 2. Age model based on all lake organic carbon radiocarbon dates (Bowen et al., 2019) from the GLAD core using the Bayesian R package BACON (Blaauw and Christen, 2011). a) Calibrated radiocarbon age probability distribution functions (blue), age model median (red line) and uncertainty (gray shading), b) comparison between all lake organic radiocarbon dates (used in this study) and the cyst-only model presented by (Bowen et al., 2019), and c) their difference. The biomarker transition at 5.5 ka in the all-lake OC model is ~200 years older than in the cyst-only model.

1. **Materials and methods**

   (a) **Lipid extraction**

We subsampled sediment core GLAD1-GSL00-1B at 30 cm intervals (approximately every 220 yrs) with each sample spanning ~1 cm (integrating ~7 yr) and samples were stored frozen at –20ºC until analysis. Sediment samples

(~10 g) were freeze-dried then homogenized with a mortar and pestle. Total lipid extracts (TLE) were obtained for each sample by immersion in 9:1 dichloromethane (DCM):methanol (MeOH) at 100°C and 1,500 psi for 15 min using Dionex ASE 350 Accelerated Solvent Extraction at the University of Southern California.

1. **GDGT quantification**

TLEs were dissolved in 99:1 hexane:isopropanol and filtered through 0.45 m PTFE (polytetrafluoroethylene) filters. Archaeol, isoGDGTs, and brGDGTs were separated using an Agilent 1260 High-Performance Liquid Chromatograph (HPLC) coupled to an Agilent 6120 Mass Spectrometer following the methods of Hopmans et al. (2016) and quantified by comparison to a C_{46} internal standard at the University of Arizona (Huguet et al., 2006). We compare the raw concentrations of summed branched and summed isoprenoidal compounds (ΣisoGDGT and ΣbrGDGT) in ng/g sediment, to assess the productivity of each compound class. Here, we also include 7-methyl isomers (isomers with methyl groups bonded in the C_7 position) in the ΣbrGDGT calculations due to their high abundance in this hypersaline environment (Wang et al., 2021).

The ACE index, a paleosalinity proxy, was calculated using the following equation from Turich and Freeman (2011):

$$ACE = \frac{\text{archaeol}}{archaeol+caldarchaeol} \times 100 \quad (1)$$

ACE indicates the proportion of GDGTs produced by halophilic Archaea and is applicable only in hypersaline environments. Note that caldarchaeol is also referred to as isoGDGT-0 or simply as GDGT-0. ACE values were converted to salinity according to the calibration of Turich and Freeman (2011), which was developed using surface sediments and suspended particulate matter from marine, hypersaline, estuarine and freshwater localities across a range of 0-250 g/L, where:

$$ACE = 0.35 \times salinity - 5.4 \quad (2)$$

The MBT_{5Me} index, a brGDGT temperature proxy, was calculated according to De Jonge et al. (2014a):

$$MBT'_{5Me} = \frac{Ia+Ib+Ic}{Ia+Ib+Ic+IIa+IIb+IIc+IIIa} \quad (3)$$

where I-III indicates the number of methyl groups (4-6), and a-c the number of cyclopentane rings (0-2). While MBT_{5Me} is most frequently used as an indicator for temperature, recent work by Martinez-Sosa et al. (2021) and Wang et al. (2021) found evidence that salinity, particularly hypersalinity, may bias temperature estimates. We convert the MBT_{5Me} values to mean annual temperature for months above freezing (MAF) using $BayMBT_0$, the Bayesian calibration of Crampton-Flood et al. (2020) available for both global surface soils and lake sediments. Martinez-Sosa et al. (2021) suggested that alkaline, saline lakes may receive greater GDGT input from surrounding soils than from in lake production. Thus, we test both the soil and lake calibrations here.

The CBT index is used as a pH indicator and was also calculated following the equation of De Jonge et al. (2014a):

$$\mathrm{CBT}' = \log_{10}\left(\frac{Ic+IIa'+IIb'+IIc'+IIIa'+IIIb'+IIIc'}{Ia+IIa+IIIa}\right) \quad (4)$$

where denotes structural isomers with methyl groups bonded in the C_6 rather than C_5 position. We calculated pH values using the global soils and lakes calibrations of Raberg et al. (2022):

$$\mathrm{CBT}' = 0.50 \times soil\ pH - 3.65 \quad (5)$$

$$\mathrm{CBT}' = 0.23 \times lake\ pH - 1.98 \quad (6)$$

As the CBT formulation in Raberg et al. (2022) included a negative sign, both calibration equations were adjusted to maintain the positive formulation of CBT (equation 4) as originally defined by De Jonge et al. (2014a).

The $\mathrm{IR}_{6\mathrm{Me}}$ index is the ratio of 6-methyl brGDGT isomers to the sum of 5- and 6-methyl brGDGT isomers, calculated according to De Jonge et al. (2014b):

$$\mathrm{IR}_{6Me} = \frac{\mathrm{IIa}'+IIb'+IIc'+IIIa'+IIIb'+IIIc'}{IIa+IIb+IIc+IIIa+IIIb+IIIc+IIa'+IIb'+IIc'+IIIa'+IIIb'+IIIc'} \quad (7)$$

The fractional cyclization (fC) index shows the proportion of brGDGTs with cyclopentane rings and is calculated according to Martinez-Sosa and Tierney (2019):

$$fC = \frac{\sum(b)+2\sum(c)+\sum\left(b'\right)+2\sum\left(c'\right)}{\sum(a)+\sum(b)+\sum(c)+\sum\left(b'\right)+\sum\left(c'\right)} \times 0.5 \quad (8)$$

The branched and isoprenoidal tetraether (BIT) index measures the proportion of branched to isoprenoidal inputs, with the isoprenoidal inputs represented only by crenarchaeol. BIT is calculated using the equation of Hopmans et al. (2004):

$$BIT = \frac{Ia+IIa+IIa'+IIIa+\mathrm{IIIa}'}{cren+Ia+IIa+IIa'+IIIa+\mathrm{IIIa}'} \quad (9)$$

However, BIT is limited in environments where crenarchaeol is a minor constituent; in such cases it may be more useful to compare the summed branched and isoprenoidal compounds using the ratio $\mathrm{R}_{\mathrm{i/b}}$:

$$R_{i/b} = \frac{\Sigma\mathrm{brGDGT}}{\Sigma\mathrm{isoGDGT}+\Sigma\mathrm{brGDGT}} \quad (10)$$

BIT was originally developed as a measure of terrestrial GDGT input to marine environments, but recent work by Xiao et al. (2016) introduced the ΣIIIa/ΣIIa ratio as a measure solely of brGDGT sourcing without including crenarchaeol:

$$\Sigma IIIa/\Sigma IIa = \frac{IIIa+\mathrm{IIIa}'}{IIa+IIa'} \quad (11)$$

Martin et al. (2020) and Ramos-Roman et al. (2022) later extended this to lacustrine environments and included the 7-methyl isomers (denoted by):

$$\Sigma IIIa/\Sigma IIa = \frac{IIIa+\mathrm{IIIa}'+\mathrm{IIIa}'''}{IIa+IIa'+IIa'''} \quad (12)$$

The proportion of GDGT-0 has previously been used to detect methanogenic archaea, which produce large quantities of GDGT-0 (Blaga et al., 2009; Damste et al., 2012; Inglis et al., 2015; Naeher et al., 2014). Although previous formulations normalize to crenarchaeol, the low abundance of this compound in GSL makes this ill-constrained. Thus, we report the fraction of GDGT-0 as:

$$\text{fGDGT-0} = \frac{\text{GDGT-0}}{\Sigma\text{isoGDGT}} \quad (13)$$

The ring index (RI) is the weighted average number of rings in the suite of measured isoGDGTs calculated using the equations of Zhang et al. (2016):

$$\text{RI}_{\text{sample}} = 0\,[\text{GDGT-0}] + 1\,[\text{GDGT-1}] + 2\,[\text{GDGT-2}] + 3\,[\text{GDGT-3}] + 4\,[\text{cren}] + 4[cren'] \quad (14)$$

where brackets indicate the concentration of an isoGDGT out of the sum of all isoGDGTs:

$$[\text{GDGT-0}] + [\text{GDGT-1}] + [\text{GDGT-2}] + [\text{GDGT-3}] + [\text{cren}] + [cren'] = 1 \quad (15)$$

RI is used to detect non-thermal influences on the TEX_{86} index, when used as a sea surface temperature (SST) proxy or for lake temperature reconstructions. Under solely thermal influences, the TEX_{86} and RI of a sample follow a predictable trend, denoted RI_{TEX} (equation not shown here). Plotting off this trend line indicates non-thermal influences on the TEX_{86} index such as anaerobic oxidation of methane or terrestrial inputs. As this is the case at GSL, we do not use TEX_{86} as a temperature proxy in GSL.

1. **Results**

   (a) **GDGTs**

We measure the individual isoGDGT and brGDGT abundances along with archaeol abundance (data available at NOAA; So et al., 2022). IsoGDGTs are dominated by isoGDGT-0 or caldarchaeol (**Figure 3a**) and we show the distribution of the remaining isoGDGTs (**Figure 3b**). ΣisoGDGT and ΣbrGDGT were similar in magnitude (**Figure 3c**). ΣisoGDGT values had a mean of 168 ng/g (1 = 56 ng/g) and ΣbrGDGT values had a mean of 117 ng/g (1 = 39 ng/g). Only 5 out of the 35 samples had ΣbrGDGT exceeding ΣisoGDGT (by <30 ng/g).

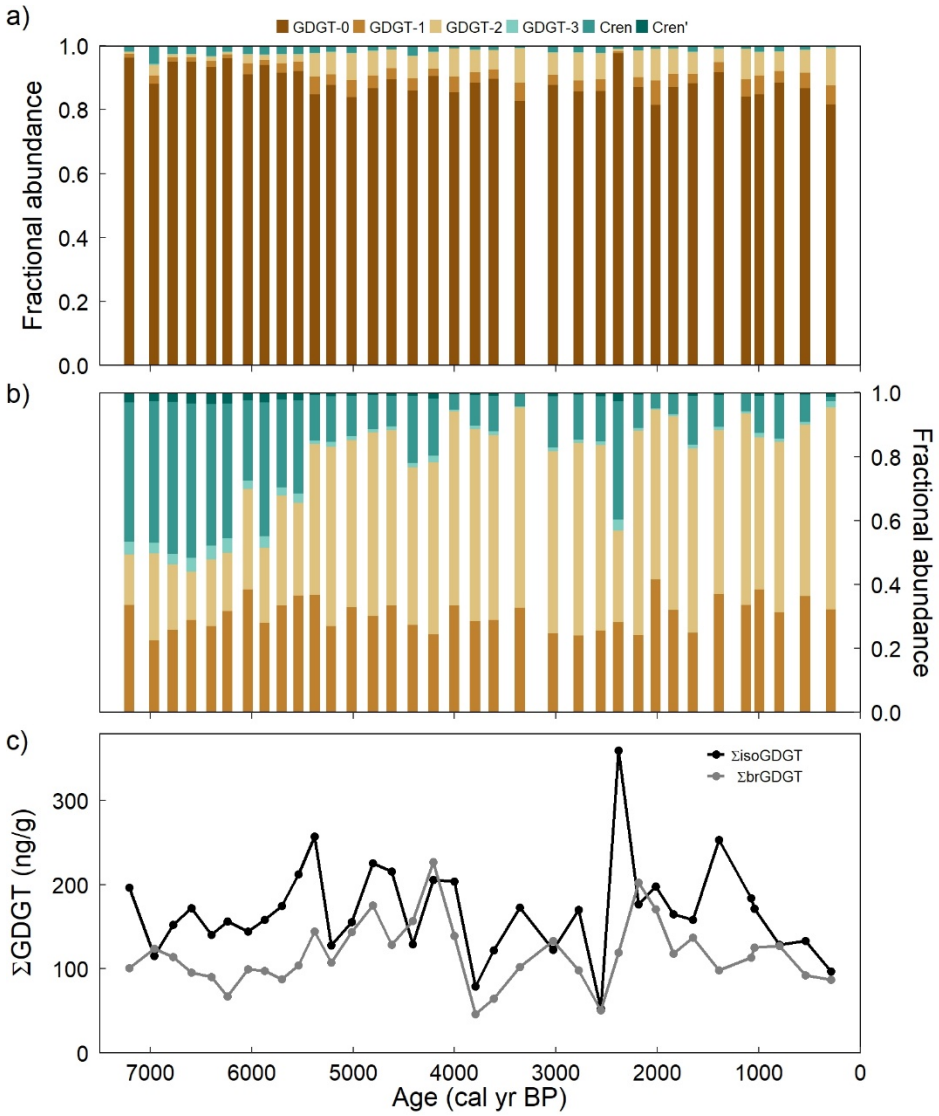

Figure 3. Change in the distribution and concentration of isoGDGTs in the GSL over the 7.2 ka record, showing a) isoGDGT proportional abundances, b) isoGDGT proportional abundances without GDGT-0, and c) isoGDGT (black) and brGDGT (gray) concentration through time.

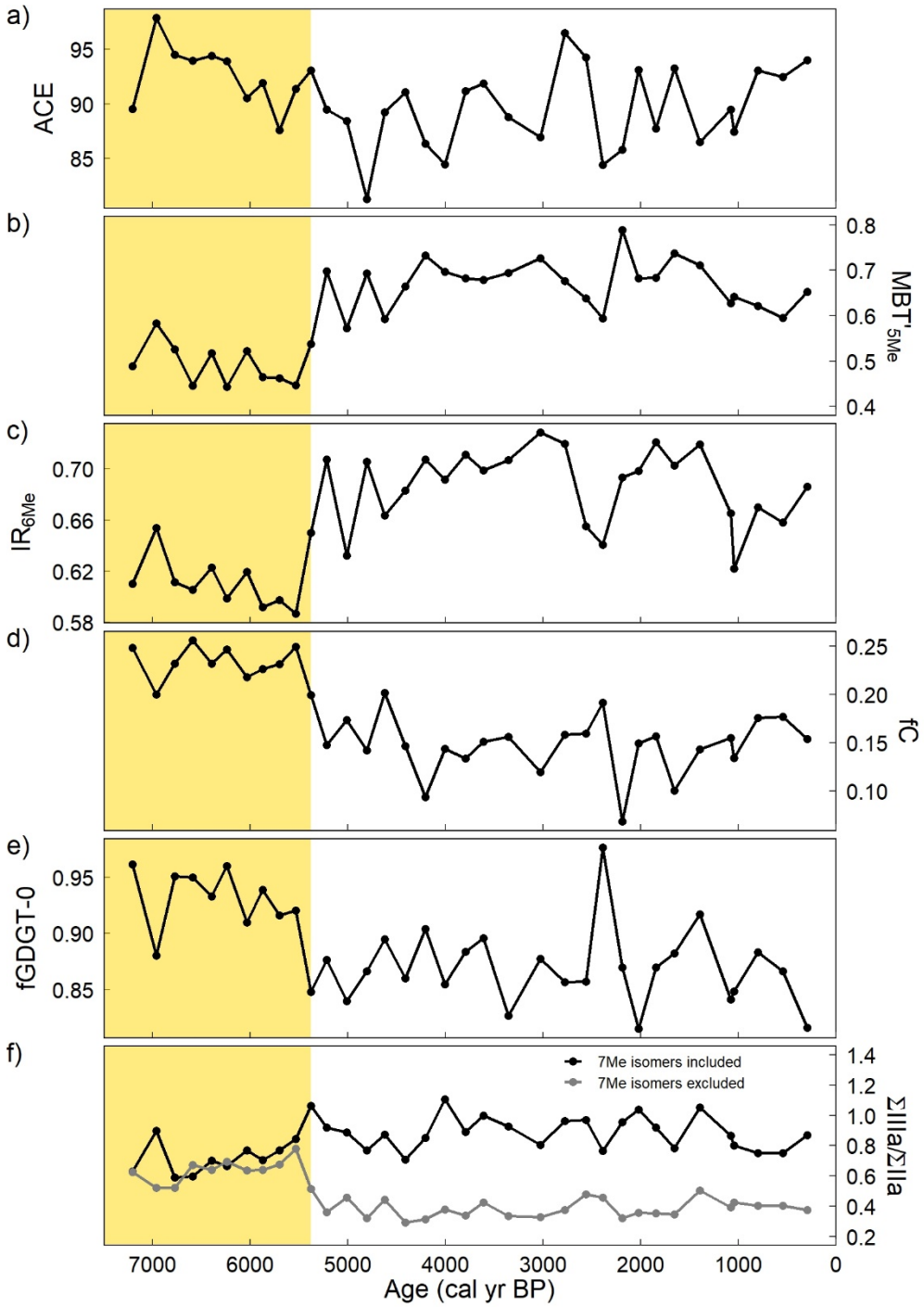

Figure 4. Temporal variations in GDGT indices showing a) ACE, b) MBT $_{5Me}$,

c) IR_{6Me}, d) fC, e) fGDGT-0, and f) ΣIIIa/ΣIIa. We see evidence for a step change in limnology at 5.5 ka, the portion of the record prior to the step change is highlighted (yellow shading).

The salinity proxy the Archaeol and Caldarchaeol Ecometric (ACE) remained relatively invariant throughout the record with a mean of 90.5 (1 = 3.7) from 7.2 ka to present (**Figure 4a**). The temperature proxy the MBT $_{5Me}$ index averaged 0.62 (1 = 0.10) from 7.2 ka to present (**Figure 4c**). MBT $_{5Me}$ showed a step shift at 5.5 ka, from a mean of 0.49 (1 = 0.05) prior to the shift to a mean of 0.67 (1 = 0.05) after. Temperature interpretations will be discussed later as many GDGT ratios show a step shift that corresponds to that in MBT $_{5Me}$ (**Figure 4**). CBT values were relatively invariant, averaging -0.01 (1 = 0.08) across the record (**Figure S1c**). IR_{6Me} values averaged 0.66 (1 = 0.04) from 7.2 ka to present, but with a noticeable step change at 5.5 ka similar to MBT $_{5Me}$ (**Figure 4b**). Prior to 5.5 ka, IR_{6Me} values averaged 0.61 (1 = 0.02) and after, the average increased to 0.69 (1 = 0.03). The fC index averaged 0.17 (1 = 0.05) from the start of the record at 7.2 ka to present. fC also featured a step shift at 5.5 ka coinciding with those of the IR and MBT $_{5Me}$, averaging 0.23 (1 = 0.02) before the shift and 0.15 (1 = 0.03) after (**Figure 4d**). The ΣIIIa/ΣIIa ratio including 7-methyl isomers remained constant over 7.2 kyr (**Figure 4f**), averaging 0.84 (1 = 0.13). However, when 7-methyl isomers are excluded, a step shift at 5.5 ka is seen, with ΣIIIa/ΣIIa averaging 0.64 (1 = 0.08) pre-shift and 0.38 (1 = 0.06) post-shift. fGDGT-0 was high with a mean of 0.89 (1 = 0.04) for the whole study period. Similar to IR_{6Me}, MBT $_{5Me}$, and fC, fGDGT-0 also saw a step change at 5.5 ka with the average being 0.93 (1 = 0.03) before and 0.87 (1 = 0.03) afterwards (**Figure 4e**).

Additional indices are relatively invariant (shown in the supplementary information). The BIT index was high (>0.90 for all samples) and varied little across 7.2 ka to present (**Figure S1f**), with a mean of 0.95 (1 = 0.02). $R_{i/b}$ averaged 0.41 (1 = 0.08) across 7.2 ka, indicating archaeal isoGDGTs to generally be more abundant than bacterial brGDGTs. The RI_{sample} remains relatively constant throughout the record (**Figure S1j**), averaging 0.23 (1 = 0.07).

1. **Discussion**

   (a) **GSL Holocene paleosalinity**

Measured ACE values for the Holocene GSL interpreted with the calibration of Turich and Freeman (2011) indicate a mean salinity of 274 g/L (1 = 11 g/L) with <50 g/L of variability for the whole record. Thus, from 7.2 ka to present, we find GSL to be hypersaline and salinity to be relatively invariant (**Figure 5**). The low variability (<50 g/L) is likely related to applying the proxy at the upper limits of the ACE index, with all samples having ACE values >80 (almost all archaeol with little caldarchaeol) and limited sensitivity to variations at high salinity. In the longer GLAD core that includes Pleistocene pluvials, the ACE proxy could be applied to study a larger range of salinities. However, in the Holocene hypersaline terminal lake system, we approach the upper limit of the

index.

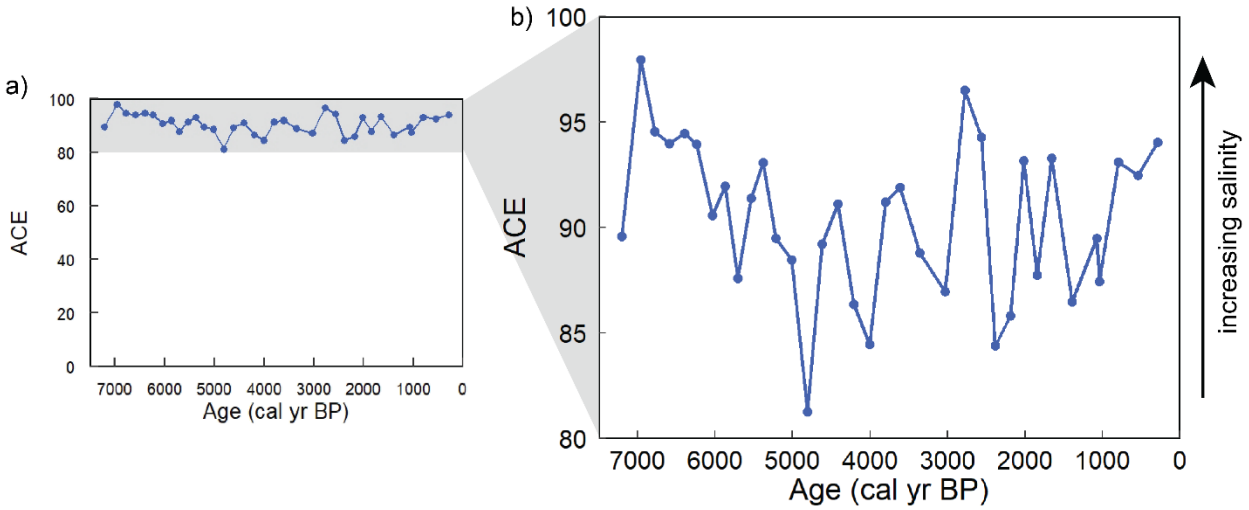

Figure 5. Variation in ACE values for the GLAD1-GSL00-1B core 7.2 ka record. a) ACE variations in the Holocene GSL. b) Adjusted y axis scale showing detailed variations in the Holocene GSL record. Arrow indicates direction of salinity increase.

Modern lake measurements indicate the North Arm brine is over 300 g/L, and the South Arm brine is close to 140 g/L (the latter being more reflective of the GSL prior to causeway separation). Historical measurements (data for 1966-2020, Rupke and McDonald, 2012) indicate the salinity range of surface samples and depth profiles in the North Arm is 250-340 g/L and the South Arm is 100-220 g/L. Although the available ACE calibration (Turich and Freeman, 2011) suggests salinities in the range of 248-295 g/L during the mid to late Holocene, these estimates appear too high, as this is higher than the modern and historical measurements for the South Arm, with such values found only in the North Arm today. Absolute salinities are approximations at present given the limited datasets for calibration and the lack of laboratory quantification standards for each of the analytes. Turich and Freeman (2011) noted that HPLC-MS measurements made in different laboratories have differential ionization of archaeol and caldarchaeol. Given the present lack of robust quantification and comparability, we interpret the ACE index as a qualitative indicator of salinity. In addition to relative response factors, the different ecologies of different aquatic communities and their limited calibration each affect the quantitative interpretation of the proxy at present. We can rule out low caldarchaeol relative response factors based on analyses with the same instrument conditions in other sedimentary archives across the full range of the ACE index (Feakins et al., 2019; Peaple et al., 2021). In the Holocene GSL, measured ACE values of 80-100 may indicate limited microbial ecology variability or a loss of sensitivity to salinity variations near the index maximum.

We can also test the ACE salinity proxy through comparison to other evidence for hypersalinity. Bowen et al. (2019) found brine shrimp cysts throughout the entire core section. In modern GSL, brine shrimp are abundant in the south arm and previous studies have identified the optimum salinity range for these shrimp to be 120-160 g/L, below which brine shrimp are limited by predation and above which by physiological stress (Great Salt Lake Salinity Advisory Committee, 2021). Though the occurrence of cysts may suggest mid-late Holocene GSL salinities of 120-160 g/L, another possibility is for cysts to be transported from elsewhere in the lake. In present day, brine shrimp cysts are found in the North Arm, where no brine shrimp can survive, likely wind-blown from the South Arm. Thus, the presence of cysts may only indicate that some parts of the lake had salinities tolerated by brine shrimp.

Overall, both ACE values and brine shrimp cyst presence indicate GSL hypersalinity over the past 7.2 kyr. However, we consider the reconstructions semi-quantitative using existing ACE calibrations. The limited variability detected by ACE and the apparent mismatch between the ACE and brine shrimp cyst salinity estimates suggests a need for additional calibration to discern the sensitivity to extreme salinity for the ACE proxy in this setting.

1. **MBT $_{\mathbf{5Me}}$ temperature record**

Using the BayMBT$_0$ lake calibration, MAF averaged 18°C (1 = 3°C) throughout the record, with a mean of 15°C (1 = 2 °C) before 5.5 ka and 20°C (1 = 2 °C) after (**Figure 6**). Lower MAF estimates resulted from the soil calibration, averaging 14°C (1 = 3°C) throughout the record, 10°C (1 = 2°C) before 5.5 ka, and 15°C (1 = 2°C) after 5.5 ka. After the step change at 5.5 ka, the soil-based calibration yields MAF estimates that closely match those of present-day Salt Lake City (15.7°C; National Centers for Environmental Information, 2022), whereas the lake-based calibration yielded temperatures that were on average 4°C too warm. A warm bias for saline lakes had previously been reported from the global lakes calibration dataset including nearby Mono Lake, California (Martinez-Sosa et al., 2021). In hypersaline, alkaline lakes, autochthonous production of brGDGTs may be low and allochthonous contributions from surrounding soils may dominate, making the soil calibration appropriate (Martinez-Sosa et al., 2021). Here, we find evidence in the Holocene GSL to corroborate this suggestion, particularly in the last 5.5 kyr, where the soil calibration yields near-modern MAF estimates.

Reconstructed temperatures increased by 5°C at 5.5 ka (**Figure 6**). Temperatures reconstructed by the soil calibration before 5.5 ka were cooler than expected when compared against modern temperatures. Previous climate records suggest the mid-Holocene to be a warm, arid period rather than a cool one (see **Section 5.4**). Having this knowledge along with the step shift we see at 5.5 ka in several GDGT indices (see **Section 5.3**), it is more likely that changes in GSL limnology at 5.5 ka affected the MBT $_{5\mathrm{Me}}$ proxy, whether through a step change in the ecological community or in the limnological conditions rather than a MAF shift of this magnitude during the Holocene. Therefore, we do not

interpret the derived temperatures for 7.2-5.5 ka (**Figure 6**, yellow shading).

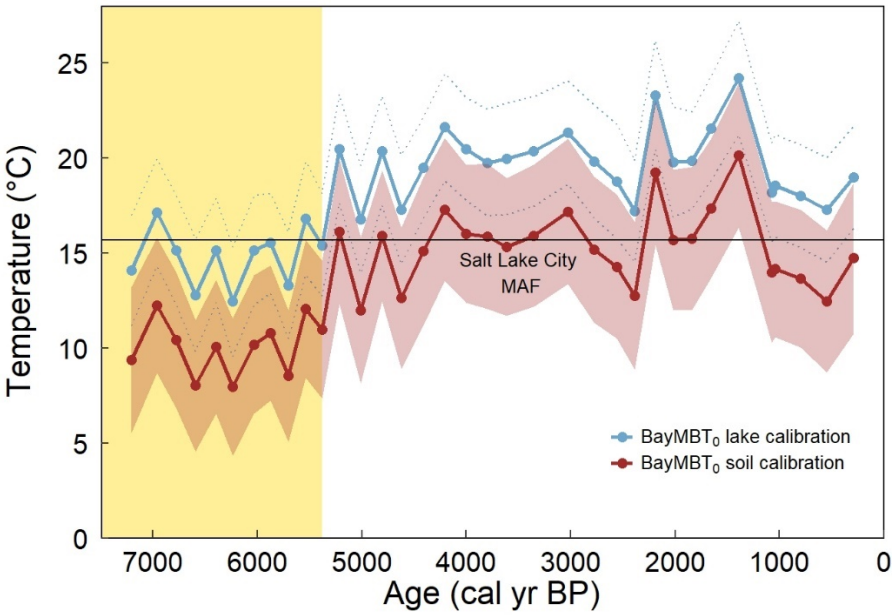

Figure 6. GSL temperature records calculated using the $BayMBT_0$ lake (blue) and soil (red) calibrations of Crampton-Flood et al. (2020) are shown along with one standard deviation uncertainty (light red envelope for soil calibration temperatures, dashed blue lines for lake calibration temperatures). The black line indicates the Salt Lake City mean annual air temperature for months above freezing (MAF). Yellow shading indicates different limnological conditions which likely affected the MBT_{5Me} proxy.

1. **Limnology shift at 5.5 ka**

Although the ACE index may be relatively insensitive to limnological change in the last 7.2 kyr given the hypersalinity of the lake, other biomarker indices show evident changes. Several GDGT proxies indicate shifts in limnological conditions at 5.5 ka (MBT_{5Me}, IR_{6Me}, fC, fGDGT-0, and ΣIIIa/ΣIIa) (**Figure 4**). We see an increase in MBT_{5Me} values at 5.5 ka (**Figure 4b**). As MBT_{5Me} is a paleotemperature proxy, these values alone would indicate increased temperatures. The increase in IR_{6Me} at this time means a proportional increase in 6-methyl brGDGT isomers (**Figure 4c**). Greater proportions of 6-methyl isomers have been linked to higher pH (De Jonge et al., 2014a; Raberg et al., 2021; Raberg et al., 2022), comparatively more aquatic production than soil production (De Jonge et al., 2014b; Kirkels et al., 2020), lower soil water content (Dang et al., 2016), and/or higher conductivity (Raberg et al., 2021). A decrease in fC is a decrease in the proportions of cyclized brGDGTs (**Figure 4d**). Less cyclization of brGDGTs have been linked to lower pH/conductivity (Raberg et al., 2021), and/or comparatively more soil production (Kirkels et al., 2020). An

increase in fGDGT-0 indicates a proportional increase in methanogenic archaea (Blaga et al., 2009; Damste et al., 2012; Inglis et al., 2015; Naeher et al., 2014) (**Figure 4e**). We also see a step increase at 5.5 ka in ΣIIIa/ΣIIa values when 7-methyl isomers are excluded (**Figure 4f**). Lower ΣIIIa/ΣIIa values indicates a lower proportion of brGDGTs with six methyl groups compared to those with five methyl groups and has been linked to increased soil inputs to lacustrine environments (Martin et al., 2020; Ramos-Roman et al., 2022). However, when 7-methyl isomers are accounted for, the ΣIIIa/ΣIIa ratio remains relatively constant. Principal component analysis (PCA) of GSL samples further supports a shift in lake conditions at 5.5 ka with samples pre- and post-5.5 ka plotting in separate clusters (**Figure S2a**).

MBT $_{5Me}$ values are low prior to this shift and, using the soil calibration, yield unrealistically cold temperatures (**Figure 6**). Lake production of brGDGTs has a 'colder' distribution than soils (Martinez-Sosa et al., 2021), thus a shift to *in situ* aquatic production might explain the observed pattern. The values pre-5.5 ka may instead represent more *in situ* lake production of brGDGTs during the middle Holocene, making it more appropriate to use the lake calibration. This is further supported by lake calibration temperatures matching more closely to modern Salt Lake City temperatures during this time. This can occur if lower lake levels prior to 5.5 ka combined with arid conditions restricted river inflows that would have brought soil-produced brGDGTs to GSL. Mixed brGDGT sourcing is possible for Holocene GSL based on its distributions of tetra-, penta-, and hexamethylated brGDGTs (Ramos-Roman et al., 2022; Russell et al., 2018) falling between those of global lakes and soils (**Figure S3, S4**), although neither pre- nor post-5.5 ka distributions can be unambiguously ascribed to a purely lake-like or soil-like signal compared to large global datasets (**Figure S2b, S4**). The PCA analysis shows that GSL has an extreme brGDGT distribution compared to global distributions, especially prior to 5.5 ka (**Figure S2b**).

Across the 5.5 ka transition, IR_{6Me} and fC increase and decrease respectively (**Figure 4c, 4d**). pH estimated using the soil calibration of Raberg et al. (2022) averaged 7.2 (1 = 0.02) and using the lake calibration averaged 8.6 (1 = 0.03). Both calibrations yield near-constant pH values throughout the whole record meaning shifts in IR_{6Me} and fC are likely not due to changes in pH. Pre-5.5 ka, higher fC could indicate higher conductivity which may reflect higher temperature and/or higher salinity, both of which align with middle Holocene aridity (see **Section 5.4**). Lower IR_{6Me} values are harder to reconcile as they would suggest lower conductivity, opposite that of fC. Aside from conductivity, low IR_{6Me} may otherwise indicate higher soil water content and/or a greater influx of organic material produced in soils. However, these factors seem secondary to pH and conductivity as controls of IR_{6Me}. Additionally, an interpretation of high soil water content or soil production would contrast with both MBT $_{5Me}$ patterns, which show greater in situ lake production pre-5.5 ka, and regional climate records, which highlight mid-Holocene aridity. We consider the well-studied and better-constrained MBT $_{5Me}$ index and the abundance of records

showing aridity at this time to be more reliable indicators of lake conditions than the relatively new IR_{6Me} index. Due to the large number of factors with potential to influence IR_{6Me} at this site, we do not interpret the exact environmental implications of the IR_{6Me} step change.

fGDGT-0 reflects the amount of methanogens in the archaeal community (Blaga et al., 2009; Damste et al., 2012; Inglis et al., 2015; Naeher et al., 2014). High fGDGT-0 values (>0.80) throughout the whole record suggest low bottom water oxygen to be a feature of Holocene GSL, but relatively higher values in the mid-Holocene (~0.95) suggest more methanogens and lower oxygen concentrations at this time compared to the late Holocene (~0.85) (**Figure 4e**). Such a change may be attributed to increased lake stratification before 5.5 ka.

The decrease in ΣIIIa/ΣIIa values with the exclusion of 7-methyl isomers would suggest greater soil input after 5.5 ka, agreeing with MBT $_{5Me}$ trends (**Figure 4f**). Throughout the 7.2 kyr record, the quantity of 7-methyl isomers is comparable to or exceeds their 5- and 6-methyl counterparts, resulting in invariant ΣIIIa/ΣIIa when these isomers are included. Wang et al. (2021) reported high abundances of 7-methyl isomers in hypersaline lakes and low amounts in freshwater lakes. The high abundance of 7-methyl isomers at hypersaline GSL may explain the trends in the different formulations of ΣIIIa/ΣIIa (**Figure 4f**). It is likely that 7-methyl brGDGTs are produced within the hypersaline lake and their high abundance obscures the signal of source change reflected in ΣIIIa/ΣIIa values when these isomers are excluded.

The coincident step shift in five GDGT indices (MBT $_{5Me}$, IR_{6Me}, fC, fGDGT-0, and ΣIIIa/ΣIIa) (**Figure 4**) suggests a change in brGDGT sourcing, lake levels, and lake chemistry marked by a change in both the bacterial and archaeal communities. Specifically, we see a shallower, possibly slightly more saline/warmer, less oxygenated/more stratified lake before 5.5 ka. Post-5.5 ka, GSL levels likely rise, soil productivity exceeds *in situ* lake productivity, and oxygen concentrations in bottom waters increase.

1. **Comparison to regional climate**

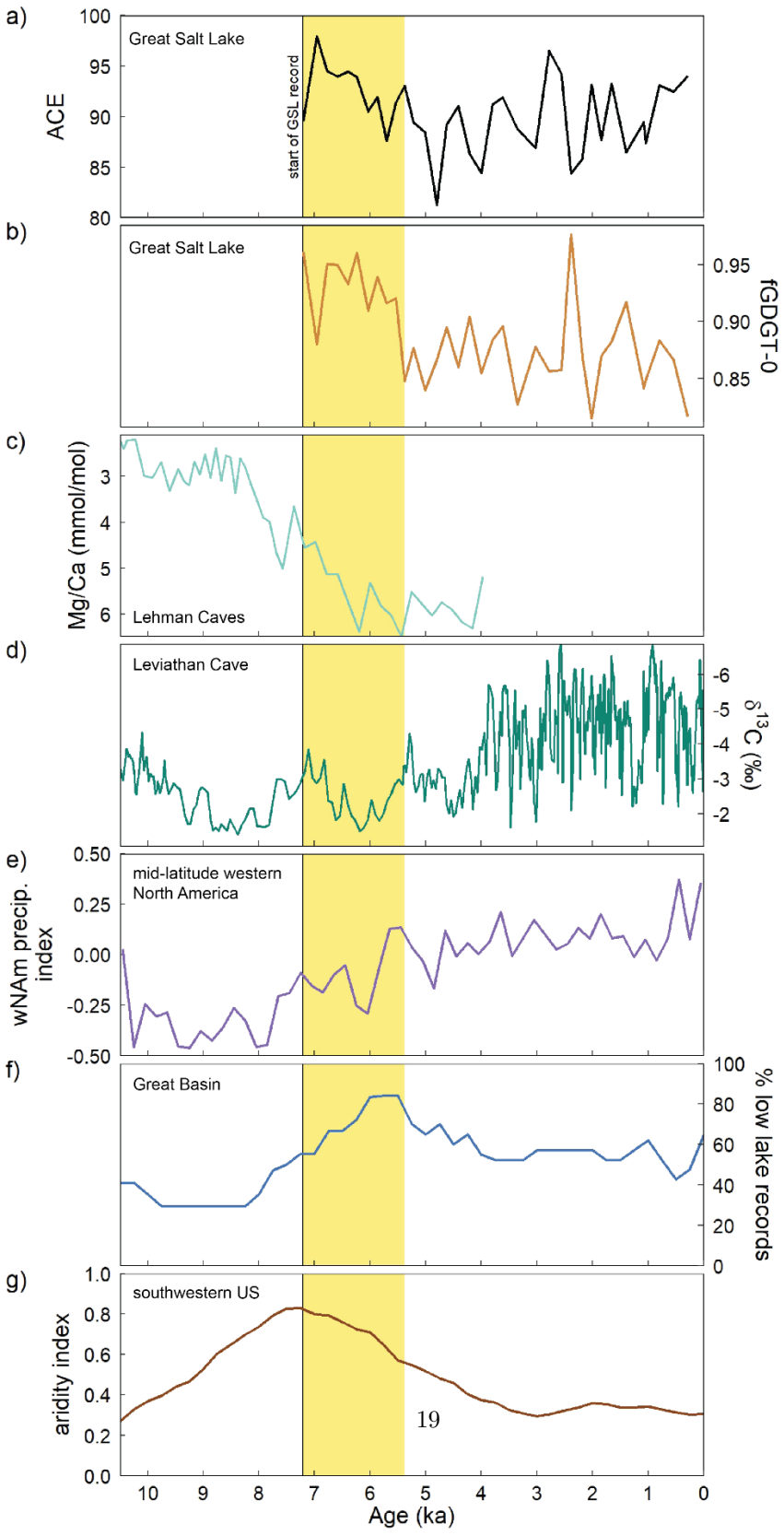
a)
Great Salt Lake
start of GSL record
ACE
100
95
90
85
80
b)
Great Salt Lake
fGDGT-0
0.95
0.90
0.85
c)
Mg/Ca (mmol/mol)
3
4
5
6
Lehman Caves
d)
Leviathan Cave
δ13C (‰)
-6
-5
-4
-3
-2
e)
mid-latitude western North America
wNAm precip. index
0.50
0.25
0.00
-0.25
-0.50
f)
Great Basin
% low lake records
100
80
60
40
20
0
g)
southwestern US
aridity index
1.0
0.8
0.6
0.4
0.2
0.0
10
9
8
7
6
5
4
3
2
1
0
Age (ka)

Figure 7. Regional paleoclimate reconstructions compilation, showing a) GSL ACE salinity (this study); b) GSL fGDGT-0 record (this study); c) Lehman Caves (NV) Mg/Ca record (Steponaitis et al., 2015); d) Leviathan Cave (NV) ^{13}C record (Lachniet et al., 2020), e) precipitation index of midlatitude western North America with high values indicating greater precipitation (Routson et al., 2022), f) percent of Great Basin lakes with low lake levels (Steponaitis et al., 2015); f) aridity index for the southwestern US with high values indicating arid conditions (Lachniet et al., 2020).

We compare select GSL biomarker records for salinity and methanogens, a measure of lake level and stratification (**Figure 7a, b**) to previously published climate records across the western US. We find evidence for low lake levels, with stratified limnology and high methanogen activity, in GSL between 7.2 to 5.5 ka (yellow shading, **Figure 7b**). Similarly, in Lehman Caves (NV) located 260 km southwest of GSL, a decrease in speleothem Mg/Ca shows increased aridity at ~8 ka (Steponaitis et al., 2015) (**Figure 7c**). In nearby Leviathan Cave (NV) 180 km southwest of GSL, a decrease in ^{13}C values at ~4 ka is interpreted as an increase in effective moisture (Lachniet et al., 2020) (**Figure 7d**). Collectively, these cave records bracket a mid-Holocene arid period from around 8-4 ka. A proxy synthesis and reanalysis effort across western North America (Routson et al., 2022) identifies a mid-latitude moisture increase in this region after 6 ka (**Figure 7e**). Preceding this moisture increase, we observe low lake levels in many Great Basin lakes (Steponaitis et al., 2015) (**Figure 7f**) as well as at small lakes in the Midwest (Shuman et al., 2002) and in the sub-alpine region of the Rocky Mountains (Shuman and Serravezza, 2017). A compilation of southwestern US climate records by Lachniet et al. (2020) also found peak aridity at 7.5 ka (**Figure 7g**). Thus, it seems likely that widespread mid-Holocene aridity in mid-latitude western North America contributed to a shallower GSL recorded from the start of this record at 7.2 ka to 5.5 ka, with a shift to wetter conditions represented locally at 5.5 ka.

Most of the precipitation in the Great Basin falls during the winter with moisture delivered by westerlies from the Pacific, and a much smaller fraction falls during the summer as part of the North American Monsoon (NAM) with moisture from the Gulf of California and eastern Pacific (Lachniet et al., 2020). Moisture from the Gulf of Mexico can also contribute to the NAM, but this rarely reaches the Great Basin (Jana et al., 2018). Changes in the incursion of the NAM and the position of westerlies over western North America have been inferred from the reanalysis of a large network of proxy data (Routson et al., 2022). They identified a strong NAM that peaked at 7 ka, coincident with weakened/northward-deflected westerlies. The latter could explain the dry mid-Holocene in the mid-latitudes, including at GSL from 7.2 to 5.5 ka, as it would have decreased delivery of Pacific moisture. Following this, in the late Holocene, a reduction in the NAM and more zonal westerly flow, resulted in wetter conditions in western North America including at GSL.

Routson et al. (2022) suggested that these changes in circulation were linked

to meridional temperature gradients. Changes in broad scale atmospheric circulation and Pacific SSTs due to high summer insolation and Laurentide ice sheet (LIS) collapse have previously been connected to Holocene shifts in the precipitation regime over the western US. Summer northern hemisphere insolation peaked in the Early Holocene ~11-10 ka and has steadily decreased up to the present (Lachniet et al., 2020). In the same time period, the LIS rapidly declined from 10-8 ka (Shuman et al., 2002), mostly having disappeared by ~7 ka (Peltier et al., 2015). Steponaitis et al. (2015) attributed the onset of mid-Holocene aridity in the Great Basin at ~8 ka to a northward displacement of winter storm tracks after the collapse of the remnant LIS. In contrast, Lachniet et al. (2020) suggested summer insolation to be the primary driver of regional climate variation. They find a connection between southwestern US drought and increased SSTs in the western tropical Pacific (WTP), warmth in the Arctic, and low Arctic sea ice, these phenomena being caused by high summer insolation. Both Steponaitis et al. (2015) and Lachniet et al. (2020) also suggest that a La Niña-like configuration of the tropical Pacific (a response to orbital forcing (Brierley et al., 2020)) may have contributed to regional aridity.

Changes in summer insolation and the LIS have also been linked to hydroclimate changes in other regions of the US. Lake and pollen records indicate a moist to dry transition in the Midwest, and a dry to moist transition in the northeast and southeast between 9 and 8 ka, attributed to the collapse of the LIS Hudson Bay Dome and the subsequent proportional increase in the influence of summer insolation (Shuman et al., 2002). In the northeast, plant wax isotopes show an increased ratio of summer to winter precipitation after 8 ka, as the LIS glacial anticyclone previously prevented northward transport of subtropical moisture during the summer (Shuman et al., 2006). From ~9-7 ka, lakes in California, the Great Basin, and the Rocky Mountains declined while those in western Canada rose. These trends reversed by ~5.7 ka, possibly due to the decline in summer insolation after the LIS melted (Shuman and Serravezza, 2017). Similarly, between 5.7-5.2 ka, lakes across central and eastern mid-latitude North America show an increase in effective moisture, which terminated mid-Holocene aridity and coincided with the end of the Holocene temperature maximum in this region (Shuman and Marsicek, 2016). A global compilation of Holocene temperature proxies ("Temperature 12K") including their age model uncertainties, places the central estimate for mid-Holocene warmth around 6.45 ka within a range of 7.65-4.95 ka (Kaufman et al., 2020).

Model studies also suggest similar patterns of mid-Holocene aridity driven by large scale climatic processes. Diffenbaugh et al. (2006) found insolation to be the primary driver of North American midcontinent aridity and model efforts by Shin et al. (2006) suggested persistent La Niña-like Pacific SST patterns (i.e. warm western tropical Pacific, cool eastern tropical Pacific). Bhattacharya et al. (2018) found both models and proxy records from the Gulf of California region indicate a weakened NAM during the last glacial and NAM strengthening as the LIS retreated and westerly storm tracks, which previously mixed in cold, dry air that weakened the NAM, were displaced/weakened. While the LIS had

largely disappeared by the middle Holocene, PMIP4-CMIP6 simulations still show enhanced seasonality and stronger monsoons in the northern hemisphere compared to preindustrial times (Brierley et al., 2020). The model dynamics support the proxy evidence for a strong NAM and weakened westerlies in the middle Holocene, leaving dry conditions in mid-latitude western North America (Routson et al., 2022). In the late Holocene, once NAM weakened, the more zonal westerlies (Routson et al., 2022) may have increased the moisture flux to the GSL region, resulting in the more mesic conditions experienced until recently.

1. Conclusions

We reconstructed a Holocene paleoclimate record for GSL using GDGT biomarker analyses of lacustrine sediments from the GLAD1-GSL00-1B sediment core spanning 7.2 ka to the present. Hypersaline conditions existed in GSL throughout the record with <50 g/L of variability, based on the ACE salinity proxy. However, Holocene GSL is near the upper limit of the ACE index (>80). Thus, sensitivity to increased salinity is inherently limited. Previous studies have indicated problems with applying the ACE index in brackish lakes (<34 g/L) at the lower limit of the proxy (Turich and Freeman, 2011). Here, we identify that in hypersaline systems, like modern Great Salt Lake we approach the upper limit of the index (ACE >80) although brine shrimp cysts in the core suggests parts of the lake remained in the 120-160 g/L range, below the theoretical upper limit of the proxy. Although relatively invariant in the mid to late Holocene, the ACE index may identify freshening of GSL during Pleistocene pluvials, and thus merits further testing on the longer sedimentary record of GSL and other western North American lakes.

When interpreting the MBT_{5Me} temperature proxy, we find the $BayMBT_0$ soil calibration yielded MAF estimates consistent with modern Salt Lake City MAF from 5.5 ka to the present. This finding is consistent with other hypersaline lakes where soil inputs may dominate over lacustrine bacterial production (Martinez-Sosa et al., 2021). Several other GDGT proxies (IR_{6Me}, fC, fGDGT-0, ΣIIIa/ΣIIa) also indicate a step shift in limnological conditions at 5.5 ka. From 7.2 to 5.5 ka, we interpret a shallower, possibly warmer/saltier lake with poorly oxygenated bottom waters. Temperature estimates using the soil calibration are unreasonably low for this dry period and this could indicate a slowdown in river supply of soil-derived brGDGTs. During this time, GSL may have received proportionally more aquatic brGDGT production, and the lake calibration yields temperature estimates similar to modern MAF. This record from GSL adds to other regional evidence for dry conditions during the mid-Holocene, from the start of the record to 5.5 ka. Based on this biomarker record, mid-Holocene lake conditions did not recur in the late Holocene. However, in the present day, GSL is drying and shifting away from its late Holocene state and approaching conditions resembling that of the mid-Holocene.

The Holocene record from this and previous studies (Spencer et al., 1984; Balch et al., 2005; Bowen et al., 2019) shows that low lake levels and hypersaline

conditions existed at GSL over the last 7.2 ka, most notably between 7.2 and 5.5 ka, which further documents the long-term record of perennial hypersaline lake conditions at GSL. Such conditions were achieved by the balance between direct precipitation and river inflow (mostly from snowmelt) and evaporation. That balance has been disrupted during the extreme decline in lake level of 7 m over the last 36 years (0.2 m/yr), from 1986 to 2022, which has reduced the surface from 8550 km^2 to 2460 km^2 (Utah Department of Natural Resources, 2022). Such rates of lake level decline are driven first by human water usage and second by climate change (Wurtsbaugh et al., 2017). The record of relatively stable conditions at GSL over the last 7.2 kyr reported here offers new baseline data on pre-anthropogenic conditions at GSL against which modern and predicted future lake conditions can be compared.

Acknowledgements

This study was supported by U.S. National Science Foundation Grant NSF-EAR-1903665 to S.F., and the Packard Fellowship for Science and Engineering to J.T. Sample material used in this project was provided by LacCore. We thank Patrick Murphy for performing GDGT analyses. We thank Yige Zhang, Gabriel Bowen, David McGee, Mark Peaple, Emily Tibbett and Annie Tamalavage for helpful discussions.

Supporting Information

Supporting Information may be found in the online version of this article.

Conflict of Interest

The authors declare no financial conflicts of interests for any author or their affiliations.

Data Availability Statement

Data files are archived at the NOAA paleoclimatology database (So et al., 2022).

References

https://www.ncei.noaa.gov/access/paleo-search/study/36833

Adams, K.D. (2007) Late holocene sedimentary environments and lake-level fluctuations at Walker Lake, Nevada, USA. Geological Society of America Bulletin 119, 126-139.10.1130/b25847.1.Bacon, S.N., Jayko, A.S., Owen, L.A., Lindvall, S.C., Rhodes, E.J., Schumer, R.A. and Decker, D.L. (2020) A 50,000-year record of lake-level variations and overflow from Owens Lake, eastern California, USA. Quaternary Science Reviews 238, 25.10.1016/j.quascirev.2020.106312.Baxter, B.K., Litchfield, C.D., Sowers, K., Griffith, J.D., DasSarma, P.A. and DasSarma, S. (2005) Microbial diversity of Great Salt Lake. Adaptation to Life at High Salt Concentrations in Archaea, Bacteria, and Eukarya 9, 9-+Belovsky, G.E., Stephens, D., Perschon, C., Birdsey, P., Paul, D., Naftz, D., Baskin, R., Larson, C., Mellison, C., Luft, J., Mosley, R., Mahon, H., Van Leeuwen, J. and Allen, D.V. (2011) The Great Salt Lake Ecosystem (Utah, USA): long

term data and a structural equation approach. Ecosphere 2, 40.10.1890/es10-00091.1.Benson, L., Kashgarian, M., Rye, R., Lund, S., Paillet, F., Smoot, J., Kester, C., Mensing, S., Meko, D. and Lindstrom, S. (2002) Holocene multidecadal and multicentennial droughts affecting Northern California and Nevada. Quaternary Science Reviews 21, 659-682.10.1016/s0277-3791(01)00048-8.Benson, L.V., Meyers, P.A. and Spencer, R.J. (1991) Change in the size of Walker Lake during the past 5000 years. Palaeogeography Palaeoclimatology Palaeoecology 81, 189-214.10.1016/0031-0182(91)90147-j.Bhattacharya, T., Tierney, J.E., Addison, J.A. and Murray, J.W. (2018) Ice-sheet modulation of deglacial North American monsoon intensification. Nature Geoscience 11, 848-+.10.1038/s41561-018-0220-7.Bird, B.W. and Kirby, M.E. (2006) An alpine lacustrine record of early Holocene North American Monsoon dynamics from Dry Lake, southern California (USA). Journal of Paleolimnology 35, 179-192.10.1007/s10933-005-8514-3.Blaauw, M. and Christen, J.A. (2011) Flexible Paleoclimate Age-Depth Models Using an Autoregressive Gamma Process. Bayesian Analysis 6, 457-474.10.1214/ba/1339616472.Blaga, C.I., Reichart, G.J., Heiri, O. and Damste, J.S.S. (2009) Tetraether membrane lipid distributions in water-column particulate matter and sediments: a study of 47 European lakes along a north-south transect. Journal of Paleolimnology 41, 523-540.10.1007/s10933-008-9242-2.Blunt, A.B. and Negrini, R.M. (2015) Lake levels for the past 19,000 years from the TL05-4 cores, Tulare Lake, California, USA: Geophysical and geochemical proxies. Quaternary International 387, 122-130.10.1016/j.quaint.2015.07.001.Bowen, G.J., Nielson, K.E. and Eglinton, T.I. (2019) Multi-substrate radiocarbon data constrain detrital and reservoir effects in Holocene sediments of the Great Salt Lake, Utah. Radiocarbon 61, 905-926.10.1017/rdc.2019.62.Brierley, C.M., Zhao, A.N., Harrison, S.P., Braconnot, P., Williams, C.J.R., Thornalley, D.J.R., Shi, X.X., Peterschmitt, J.Y., Ohgaito, R., Kaufman, D.S., Kageyama, M., Hargreaves, J.C., Erb, M.P., Emile-Geay, J., D'Agostino, R., Chandan, D., Carre, M., Bartlein, P.J., Zheng, W.P., Zhang, Z.S., Zhang, Q., Yang, H., Volodin, E.M., Tomas, R.A., Routson, C., Peltier, W.R., Otto-Bliesner, B., Morozova, P.A., McKay, N.P., Lohmann, G., Legrande, A.N., Guo, C.C., Cao, J., Brady, E., Annan, J.D. and Abe-Ouchi, A. (2020) Large-scale features and evaluation of the PMIP4-CMIP6 midHolocene simulations. Climate of the Past 16, 1847-1872.10.5194/cp-16-1847-2020.Briggs, R.W., Wesnousky, S.G. and Adams, K.D. (2005) Late Pleistocene and late Holocene lake highstands in the Pyramid Lake subbasin of Lake Lahontan, Nevada, USA. Quaternary Research 64, 257-263.10.1016/j.yqres.2005.02.011.Crampton-Flood, E.D., Tierney, J.E., Peterse, F., Kirkels, F. and Damste, J.S.S. (2020) BayMBT: A Bayesian calibration model for branched glycerol dialkyl glycerol tetraethers in soils and peats. Geochimica Et Cosmochimica Acta 268, 142-159.10.1016/j.gca.2019.09.043.Damste, J.S.S., Ossebaar, J., Schouten, S. and Verschuren, D. (2012) Distribution of tetraether lipids in the 25-ka sedimentary record of Lake Challa: extracting reliable TEX86 and MBT/CBT palaeotemperatures from an equatorial African lake. Quaternary Science Reviews 50, 43-54.10.1016/j.quascirev.2012.07.001.Dang, X.Y., Yang, H.,

Naafs, B.D.A., Pancost, R.D. and Xie, S.C. (2016) Evidence of moisture control on the methylation of branched glycerol dialkyl glycerol tetraethers in semi-arid and arid soils. Geochimica Et Cosmochimica Acta 189, 24-36.10.1016/j.gca.2016.06.004.Dawson, K.S., Freeman, K.H. and Macalady, J.L. (2012) Molecular characterization of core lipids from halophilic archaea grown under different salinity conditions. Organic Geochemistry 48, 1-8.10.1016/j.orggeochem.2012.04.003.De Jonge, C., Hopmans, E.C., Zell, C.I., Kim, J.H., Schouten, S. and Damste, J.S.S. (2014a) Occurrence and abundance of 6-methyl branched glycerol dialkyl glycerol tetraethers in soils: Implications for palaeoclimate reconstruction. Geochimica Et Cosmochimica Acta 141, 97-112.10.1016/j.gca.2014.06.013.De Jonge, C., Stadnitskaia, A., Hopmans, E.C., Cherkashov, G., Fedotov, A. and Damste, J.S.S. (2014b) In situ produced branched glycerol dialkyl glycerol tetraethers in suspended particulate matter from the Yenisei River, Eastern Siberia. Geochimica Et Cosmochimica Acta 125, 476-491.10.1016/j.gca.2013.10.031.Diffenbaugh, N.S., Ashfaq, M., Shuman, B., Williams, J.W. and Bartlein, P.J. (2006) Summer aridity in the United States: Response to mid-Holocene changes in insolation and sea surface temperature. Geophysical Research Letters 33, 5.10.1029/2006gl028012.Dinter, D., Haskell, B., Valero-Garcés, B., Schnurrenberger, D., Heil, C., Dean, W. and Kruger, N. (2000) GLAD1, GSL SITE 1, in: Schnurrenberger, D., Haskell, B. (Eds.), Initial Reports of the Global Lakes Drilling Program. University of Arizona; Limnological Research Center, University of Minnesota; Northern Arizona University; University of Utah; United States Geological Survey; University of Rhode Island, Graduate School of Oceanography, pp. 12-17Enzel, Y., Cayan, D.R., Anderson, R.Y. and Wells, S.G. (1989) Atmospheric circulation during Holocene lake stands in the Mojave Desert - Evidence of regional climate change. Nature 341, 44-47.10.1038/341044a0.Feakins, S.J., Wu, M.S., Ponton, C. and Tierney, J.E. (2019) Biomarkers reveal abrupt switches in hydroclimate during the last glacial in southern California. Earth and Planetary Science Letters 515, 164-172.10.1016/j.epsl.2019.03.024.Goebel, T., Hockett, B., Rhode, D. and Graf, K. (2021) Prehistoric human response to climate change in the Bonneville basin, western North America: The Bonneville Estates Rockshelter radiocarbon chronology. Quaternary Science Reviews 260, 23.10.1016/j.quascirev.2021.106930.Great Salt Lake Salinity Advisory Committee (2021) Influence of Salinity on the Resources and Uses of Great Salt Lake, Utah Geological Survey Open-File Report. Utah Geological Survey.10.34191/OFR-736.He, Y.X., Wang, H.Y., Meng, B.W., Li, H., Zho, A.F., Song, M., Kolpakova, M., Kriyonogov, S., Liu, W.G. and Liu, Z.H. (2020) Appraisal of alkenone- and archaeal ether-based salinity indicators in mid-latitude Asian lakes. Earth and Planetary Science Letters 538, 10.10.1016/j.epsl.2020.116236.Hopmans, E.C., Schouten, S. and Damste, J.S.S. (2016) The effect of improved chromatography on GDGT-based palaeoproxies. Organic Geochemistry 93, 1-6.10.1016/j.orggeochem.2015.12.006.Hopmans, E.C., Weijers, J.W.H., Schefuss, E., Herfort, L., Damste, J.S.S. and Schouten, S. (2004) A novel proxy for terrestrial organic matter in sediments based on branched and isoprenoid tetraether lipids. Earth and Planetary Sci-

ence Letters 224, 107-116.10.1016/j.epsl.2004.05.012.Huguet, C., Hopmans, E.C., Febo-Ayala, W., Thompson, D.H., Damste, J.S.S. and Schouten, S. (2006) An improved method to determine the absolute abundance of glycerol dibiphytanyl glycerol tetraether lipids. Organic Geochemistry 37, 1036-1041.10.1016/j.orggeochem.2006.05.008.Inglis, G.N., Farnsworth, A., Lunt, D., Foster, G.L., Hollis, C.J., Pagani, M., Jardine, P.E., Pearson, P.N., Markwick, P., Galsworthy, A.M.J., Raynham, L., Taylor, K.W.R. and Pancost, R.D. (2015) Descent toward the Icehouse: Eocene sea surface cooling inferred from GDGT distributions. Paleoceanography 30, 1000-1020.10.1002/2014pa002723.Jagniecki, E., Rupke, A., Kirby, S. and Inkenbrandt, P. (2021) Salt crust, brine, and marginal groundwater of Great Salt Lake's North arm (2019-2021), Utah Geological Survey Report of Investigation. Utah Geological Survey, Salt Lake City, UT, USA.10.34191/RI-283.Jana, S., Rajagopalan, B., Alexander, M.A. and Ray, A.J. (2018) Understanding the Dominant Sources and Tracks of Moisture for Summer Rainfall in the Southwest United States. Journal of Geophysical Research-Atmospheres 123, 4850-4870.10.1029/2017jd027652.Jewell, P.W. (2021) Historic low stand of Great Salt Lake, Utah: I Mass balance model and origin of the deep brine layer. Sn Applied Sciences 3, 16.10.1007/s42452-021-04691-5.Jones, B.F., Naftz, D.L., Spencer, R.J. and Oviatt, C.G. (2009) Geochemical Evolution of Great Salt Lake, Utah, USA. Aquatic Geochemistry 15, 95-121.10.1007/s10498-008-9047-y.Kaufman, D., McKay, N., Routson, C., Erb, M., Datwyler, C., Sommer, P.S., Heiri, O. and Davis, B. (2020) Holocene global mean surface temperature, a multi-method reconstruction approach. Scientific Data 7, 13.10.1038/s41597-020-0530-7.Kirby, M.E., Feakins, S.J., Hiner, C.A., Fantozzi, J., Zimmerman, S.R.H., Dingemans, T. and Mensing, S.A. (2014) Tropical Pacific forcing of Late-Holocene hydrologic variability in the coastal southwest United States. Quaternary Science Reviews 102, 27-38.10.1016/j.quascirev.2014.08.005.Kirby, M.E., Lund, S.P., Anderson, M.A. and Bird, B.W. (2007) Insolation forcing of Holocene climate change in Southern California: a sediment study from Lake Elsinore. Journal of Paleolimnology 38, 395-417.10.1007/s10933-006-9085-7.Kirkels, F., Ponton, C., Galy, V., West, A.J., Feakins, S.J. and Peterse, F. (2020) From Andes to Amazon: Assessing Branched Tetraether Lipids as Tracers for Soil Organic Carbon in the Madre de Dios River System. Journal of Geophysical Research-Biogeosciences 125, 18.10.1029/2019jg005270.Lachniet, M.S., Asmerom, Y., Polyak, V. and Denniston, R. (2020) Great Basin Paleoclimate and Aridity Linked to Arctic Warming and Tropical Pacific Sea Surface Temperatures. Paleoceanography and Paleoclimatology 35, 22.10.1029/2019pa003785.Macalady, J.L., Vestling, M.M., Baumler, D., Boekelheide, N., Kaspar, C.W. and Banfield, J.F. (2004) Tetraether-linked membrane monolayers in Ferroplasma spp: a key to survival in acid. Extremophiles 8, 411-419.10.1007/s00792-004-0404-5.Martin, C., Menot, G., Thouveny, N., Peyron, O., Andrieu-Ponel, V., Montade, V., Davtian, N., Reille, M. and Bard, E. (2020) Early Holocene Thermal Maximum recorded by branched tetraethers and pollen in Western Europe (Massif Central, France). Quaternary Science Reviews 228, 21.10.1016/j.quascirev.2019.106109.Martinez-Sosa, P. and Tierney, J.E.

(2019) Lacustrine brGDGT response to microcosm and mesocosm incubations. Organic Geochemistry 127, 12-22.10.1016/j.orggeochem.2018.10.011.Martinez-Sosa, P., Tierney, J.E., Stefanescu, I.C., Crampton-Flood, E.D., Shuman, B.N. and Routson, C. (2021) A global Bayesian temperature calibration for lacustrine brGDGTs. Geochimica Et Cosmochimica Acta 305, 87-105.10.1016/j.gca.2021.04.038.Mensing, S.A., Sharpe, S.E., Tunno, I., Sada, D.W., Thomas, J.M., Starratt, S. and Smith, J. (2013) The Late Holocene Dry Period: multiproxy evidence for an extended drought between 2800 and 1850 cal yr BP across the central Great Basin, USA. Quaternary Science Reviews 78, 266-282.10.1016/j.quascirev.2013.08.010.Moser, K.A. and Kimball, J.P. (2009) A 19,000-year record of hydrologic and climatic change inferred from diatoms from Bear Lake, Utah and Idaho, Paleoenvironments of Bear Lake, Utah and Idaho, and Its Catchment. Geological Soc Amer Inc, Boulder, pp. 229-246.Naeher, S., Niemann, H., Peterse, F., Smittenberg, R.H., Zigah, P.K. and Schubert, C.J. (2014) Tracing the methane cycle with lipid biomarkers in Lake Rotsee (Switzerland). Organic Geochemistry 66, 174-181.10.1016/j.orggeochem.2013.11.002.Naftz, D. (2017) Inputs and Internal Cycling of Nitrogen to a Causeway Influenced, Hypersaline Lake, Great Salt Lake, Utah, USA. Aquatic Geochemistry 23, 199-216.10.1007/s10498-017-9318-6.National Centers for Environmental Information (2022) Time series- monthly GHCN v3 mean temperature- Salt Lake Cit (United States of America), Null, S.E. and Wurtsbaugh, W.A. (2020) Water Development, Consumptive Water Uses, and the Great Salt Lake, in: Baxter, B.K., Butler, J.K. (Eds.), Great Salt Lake Biology, A Terminal Lake in a Time of Change. Springer Nature Switzerland AG, Cham, Switzerland, pp. 1-21.Oviatt, C.G., Atwood, G. and Thompson, R.S. (2021) History of Great Salt Lake, Utah, USA: since the Termination of Lake Bonneville, in: Rosen, M.R., Finkelstein, D.B., Park Boush, L., Pla-Pueyo, S. (Eds.), Limnogeology: Progress, Challenges and Opportunities : A Tribute to Elizabeth Gierlowski-Kordesch. Springer International Publishing, Cham, pp. 233-271.Oviatt, C.G., Madsen, D.B., Miller, D.M., Thompson, R.S. and McGeehin, J.P. (2015) Early Holocene Great Salt Lake, USA. Quaternary Research 84, 57-68.10.1016/j.yqres.2015.05.001.Peaple, M.D., Bhattacharya, T., Lowenstein, T., McGee, D., Olson, K., Stroup, J.S., Tierney, J.E. and Feakins, S.J. (2022) Biomarker and pollen evidence for late Pleistocene pluvials in the Mojave Desert. Earth and Space Science Open Archive, 45.doi:10.1002/essoar.10511222.1.Peaple, M.D., Tierney, J.E., McGee, D., Lowenstein, T.K., Bhattacharya, T. and Feakins, S.J. (2021) Identifying plant wax inputs in lake sediments using machine learning. Organic Geochemistry 156, 11.10.1016/j.orggeochem.2021.104222.Peltier, W.R., Argus, D.F. and Drummond, R. (2015) Space geodesy constrains ice age terminal deglaciation: The global ICE-6G_C (VM5a) model. Journal of Geophysical Research-Solid Earth 120, 450-487.10.1002/2014jb011176.Perry, K.D., Crosman, E.T. and Hoch, S.W. (2019) Results of the Great Salt Lake Dust Plume Study (2016-2018). University of Utah, Salt Lake City, UT, USARaberg, J.H., Harning, D.J., Crump, S.E., de Wet, G., Blumm, A., Kopf, S., Geirsdottir, A., Miller, G.H. and Sepulveda, J. (2021) Revised fractional

abundances and warm-season temperatures substantially improve brGDGT calibrations in lake sediments. Biogeosciences 18, 3579-3603.10.5194/bg-18-3579-2021.Raberg, J.H., Miller, G.H., Geirsdottir, A. and Sepulveda, J. (2022) Near-universal trends in brGDGT lipid distributions in nature. Science Advances 8, 12.10.1126/sciadv.abm7625.Ramirez, R. (2022) Great Salt Lake is 'in trouble' as level falls to lowest on record for second year in a row. CNNRamos-Roman, M.J., De Jonge, C., Magyari, E., Veres, D., Ilvonen, L., Develle, A.L. and Seppa, H. (2022) Lipid biomarker (brGDGT)- and pollen-based reconstruction of temperature change during the Middle to Late Holocene transition in the Carpathians. Global and Planetary Change 215, 13.10.1016/j.gloplacha.2022.103859.Routson, C.C., Erb, M.P. and McKay, N.P. (2022) High Latitude Modulation of the Holocene North American Monsoon. Geophysical Research Letters 49, 10.10.1029/2022gl099772.Rupke, A. and McDonald, A. (2012) Great Salt Lake brine chemistry database, 1966-2011, Utah Geological Survey Open-File Report. Utah Geological Survey, Salt Lake City Utah, p. 7.10.34191/OFR-596.Russell, J.M., Hopmans, E.C., Loomis, S.E., Liang, J. and Damste, J.S.S. (2018) Distributions of 5-and 6-methyl branched glycerol dialkyl glycerol tetraethers (brGDGTs) in East African lake sediment: Effects of temperature, pH, and new lacustrine paleotemperature calibrations. Organic Geochemistry 117, 56-69.10.1016/j.orggeochem.2017.12.003.Schouten, S., Hopmans, E.C. and Damste, J.S.S. (2013) The organic geochemistry of glycerol dialkyl glycerol tetraether lipids: A review. Organic Geochemistry 54, 19-61.10.1016/j.orggeochem.2012.09.006.Shin, S.I., Sardeshmukh, P.D., Webb, R.S., Oglesby, R.J. and Barsugli, J.J. (2006) Understanding the mid-Holocene climate. Journal of Climate 19, 2801-2817.10.1175/jcli3733.1.Shope, C.L. and Angeroth, C.E. (2015) Calculating salt loads to Great Salt Lake and the associated uncertainties for water year 2013; updating a 48 year old standard. Science of the Total Environment 536, 391-405.10.1016/j.scitotenv.2015.07.015.Shuman, B., Bartlein, P., Logar, N., Newby, P. and Webb, T. (2002) Parallel climate and vegetation responses to the early Holocene collapse of the Laurentide Ice Sheet. Quaternary Science Reviews 21, 1793-1805.10.1016/s0277-3791(02)00025-2.Shuman, B., Huang, Y.S., Newby, P. and Wang, Y. (2006) Compound-specific isotopic analyses track changes in seasonal precipitation regimes in the Northeastern United States at ca 8200cal yrBP. Quaternary Science Reviews 25, 2992-3002.10.1016/j.quascirev.2006.02.021.Shuman, B.N. and Marsicek, J. (2016) The structure of Holocene climate change in mid-latitude North America. Quaternary Science Reviews 141, 38-51.10.1016/j.quascirev.2016.03.009.Shuman, B.N. and Serravezza, M. (2017) Patterns of hydroclimatic change in the Rocky Mountains and surrounding regions since the last glacial maximum. Quaternary Science Reviews 173, 58-77.10.1016/j.quascirev.2017.08.012.So, R., Lowenstein, T., Jagniecki, E., Tierney, J.E. and Feakins, S.J. (2022) Great Salt Lake, GDGTs from the mid- to late Holocene [Dataset], NOAA National Centers for Environmental Information. .Sorensen, E.D., Hoven, H.M. and Neill, J. (2020) Great Salt Lake Shorebirds, Their Habitats,and Food Base, in: Baxter, B.K., Butler, J.K. (Eds.), Great Salt Lake Biology, A Terminal Lake in a Time of Change. Springer

Nature Switzerland AG, Cham, Switzerland, pp. 263-309.Stefanescu, I.C., Shuman, B.N. and Tierney, J.E. (2021) Temperature and water depth effects on brGDGT distributions in sub-alpine lakes of mid-latitude North America. Organic Geochemistry 152, 15.10.1016/j.orggeochem.2020.104174.Steponaitis, E., Andrews, A., McGee, D., Quade, J., Hsieh, Y.T., Broecker, W.S., Shuman, B.N., Burns, S.J. and Cheng, H. (2015) Mid-Holocene drying of the US Great Basin recorded in Nevada speleothems. Quaternary Science Reviews 127, 174-185.10.1016/j.quascirev.2015.04.011.Stine, S. (1990) Late Holocene fluctuations of Mono Lake, eastern California. Palaeogeography Palaeoclimatology Palaeoecology 78, 333-&.10.1016/0031-0182(90)90221-r.Teixidor, P., Grimalt, J.O., Pueyo, J.J. and Rodriguezvalera, F. (1993) Isopranylglycerol diethers in nonalkaline evaporitic environments. Geochimica Et Cosmochimica Acta 57, 4479-4489.10.1016/0016-7037(93)90497-k.Turich, C. and Freeman, K.H. (2011) Archaeal lipids record paleosalinity in hypersaline systems. Organic Geochemistry 42, 1147-1157.10.1016/j.orggeochem.2011.06.002.United States Geological Survey (2022a) Bear River near Corinne, UT (10126000), National Water DashboardUnited States Geological Survey (2022b) Great Salt Lake at Saltair Harbor, UT (10010000), National Water DashboardWang, H.Y., Liu, W.G., He, Y.X., Zhou, A.F., Zhao, H., Liu, H., Cao, Y.N., Hu, J., Meng, B.W., Jiang, J.W., Kolpakova, M., Krivonogov, S. and Liu, Z.H. (2021) Salinity-controlled isomerization of lacustrine brGDGTs impacts the associated MBT5ME terrestrial temperature index. Geochimica Et Cosmochimica Acta 305, 33-48.10.1016/j.gca.2021.05.004.Wang, H.Y., Liu, W.G., Zhang, C.L.L., Jiang, H.C., Dong, H.L., Lu, H.X. and Wang, J.X. (2013) Assessing the ratio of archaeol to caldarchaeol as a salinity proxy in highland lakes on the northeastern Qinghai-Tibetan Plateau. Organic Geochemistry 54, 69-77.10.1016/j.orggeochem.2012.09.011.Wurtsbaugh, W.A., Miller, C., Null, S.E., DeRose, R.J., Wilcock, P., Hahnenberger, M., Howe, F. and Moore, J. (2017) Decline of the world's saline lakes. Nature Geoscience 10, 816-+.10.1038/ngeo3052.Xiao, W.J., Wang, Y.H., Zhou, S.Z., Hu, L.M., Yang, H. and Xu, Y.P. (2016) Ubiquitous production of branched glycerol dialkyl glycerol tetraethers (brGDGTs) in global marine environments: a new source indicator for brGDGTs. Biogeosciences 13, 5883-5894.10.5194/bg-13-5883-2016.Zhang, Y.G., Pagani, M. and Wang, Z.R. (2016) Ring Index: A new strategy to evaluate the integrity of TEX86 paleothermometry. Paleoceanography 31, 220-232.10.1002/2015pa002848.